Catalysis Today 181 (2012) 82–88

Contents lists available at ScienceDirect

Catalysis Today

journal homepage: www.elsevier.com/locate/cattod

On the mechanism of photocatalytic CO_2 reduction with water in the gas phase

Deniz Uner*, Mert Mehmet Oymak

Middle East Technical University, Chemical Engineering Department, Ankara, 06531, Turkey

ARTICLE INFO

Article history:
Received 15 March 2011
Received in revised form 31 May 2011
Accepted 21 June 2011
Available online 28 July 2011

Keywords:
Artificial photosynthesis
TiO_2
Pt
Hydrogen spillover

ABSTRACT

The mechanism of photocatalytic reduction of CO_2 with H_2O over Pt–TiO_2 films produced by the sol–gel deposition over glass beads was investigated. The accumulation of significant amount of carbonaceous intermediate on the surface followed by deactivation indicated the rate limiting reaction is the water splitting reaction, similar to the natural photosynthetic systems. When gas phase hydrogen was allowed in the system, the carbonaceous intermediates were converted to methane at rates higher than the artificial photosynthesis conditions. In the presence of hydrogen, formation of methane reaction proceeded in the dark albeit at lower rates. The progress of the reaction is very similar to the natural photosynthetic reactions however the rates are seven orders of magnitude slower than the reactions in the natural photosynthetic processes. Furthermore, the role of spilled over hydrogen in the reaction was also demonstrated.

1. Introduction

CO_2 reduction to hydrocarbons by harvesting solar energy is a promising approach since it may be the candidate to the solution of two problems: high CO_2 levels in the atmosphere which could not be compensated by CO_2 fixation cycles and future world fuel crisis which is inevitable due to long formation times of coal, natural gas or oil. In this paper, we report a comparative study of photocatalytic reduction of CO_2 with water and H_2 over sol–gel coated TiO_2 films promoted with Pt.

One of the pioneering works on CO_2 hydrogenation to methane was reported by Sabatier and Serenders in 1902 ([1] and references therein). In recent years, the need for CO_2 mitigation prompted new studies on catalyst and process development for CO_2 based products. Very high methanation activities are reported for Ru doped Ceria, reasonable levels of methane production can be observed at temperatures as low as 300 K [1]. Ru is reported to be a very active catalyst, highest activity of hydrogenation of CO_2 to formic acid in a solution of triethylamine and ethanol was achieved at 80 °C [2]. The mechanism of CO_2 hydrogenation is still being debated: some studies report that the CO_2 hydrogenation proceeded similar to CO hydrogenation with an initial oxygen elimination step from the molecule via a surface formate intermediate over Ni/ZrO_2 catalysts [3], while some other reports indicate that CO and CO_2 hydrogenation reactions take place via different paths [1]. Over Fe and Co based Fischer Tropsch catalysts, it was observed that when the CO amounts in the feed gas (composed of CO, CO_2 and H_2) decreased, the FT product-distribution shifted exclusively to methane [4]. Later studies on K promoted F catalysts, the same group reported that the reverse water–gas shift reaction imposed a thermodynamic limit to conversions and therefore selectivity, supporting their arguments with a mathematical model [5].

Not just the catalyst, but also the reactor type influences the product distribution and selectivity. Later studies on Group VIII catalysts indicated that the product distribution and site time yields are strong functions of the reactor type: among fixed bed, fluidized bed and slurry reactor types, fluidized bed and slurry type reactor performances better than the fixed bed reactor for CO_2 conversions and hydrocarbon selectivities [6]. These findings indicate that the micromixing conditions impose significant influence over the selectivities; a topic which is not as broadly covered by the catalysis community as it is needed. The catalyst structure examined along the length of a packed bed reactor revealed that the catalysts at the inlet of the reactor undergone phase transformations while at the exit the carbide formations deactivated the catalyst [7]. All of these indicate the complexity of the reaction scheme, and the need to understand not just the catalyst and its microstructure, but also the need to tailor the operating conditions for higher selectivities towards the desired products.

Over Rh/SiO_2 catalysts, it was observed that the metal loading had a significant effect of the CO_2 hydrogenation selectivity: over 1% Rh/SiO_2 catalysts the selectivity of the CO_2 reaction was towards CO, resulting from the formation of Rh carbonyl clusters stabilized by OH groups on the surface of silica, while the large particles yielded mainly methane due to the low amount of silanol groups

* Corresponding author. Tel.: +90 312 210 2601; fax: +90 312 210 2600.
E-mail address: uner@metu.edu.tr (D. Uner).

0920-5861/$ – see front matter © 2011 Elsevier B.V. All rights reserved.
doi:10.1016/j.cattod.2011.06.019

Table 1
Water splitting reaction rates on TiO_2 photocatalysts.

Photocatalyst	H_2 production rate ($\mu mol/g_{cat}$-h)	Initial H_2 production rate[a] ($\mu mol/g_{cat}$-h)	O_2 production rate ($\mu mol/g_{cat}$-h)	Conditions	References
1% Degussa P25 SCR[b] SO_4	2.72	1.6	20.64	TiO_2 initial concentration. 0.75 g/l, 2 mM $Ce_2(SO_4)_3$ pH = 1, T = 20 °C	[33]
Fe (1.2 wt.%) doped TiO_2	15.5	–	–	Distilled water	[34]
Rh/TiO_2 (MCB®)	1497	1497	748.5	10 wt.% NaOH soln.	[35]
Pt/TiO_2-A1 + TiO_2-R2 mix[c].	360	240	180	40 mmol NaI, pH = 11, 0.5 wt.% Pt loading	[36]
Au/TiO_2 – P25	7200	–	4200	1 vol.% MeOH, 2 wt.% Au loading	[37]
Au/FP5[d]	52.4	110	–	Distilled water, FP5 xylene/pyridine = 8/2	[38]
Au/FP5[d]	7890	7890	–	6 vol.% MeOH, FP5 xylene/pyridine = 8/2	[38]
1% Pt/TiO_2	3000	3000	–	Pure ethanol, T = 71 °C	[39]

[a] Converted from line graph using initial data.
[b] Soft Chemical Reduction.
[c] A:Anatase R:Rutile.
[d] Flame Spray Pyrolysis.

adjacent to Rh sites over large particles inhibited the formation of Rh carbonyls [8].

The adsorption of CO_2 over TiO_2 is also one of the challenges of the scientific community. The adsorption sites, the O–C–O bond angle upon adsorption, bending induced changes in the LUMO of the molecule and the resultant change in the electron transfer to the adsorbed molecule is very nicely reviewed in a recent article [9]. In summary, it was reported that CO_2 adsorption occurred at five coordinate Ti^{+4} sites and oxygen vacant sites created by vacuum annealing on TiO_2 (1 1 0) single crystals [10]. According to DFT studies on triplet defect-free clusters, CO_2 and stoichiometric TiO_2 anatase do not lead to charge transfer and form CO_2^{*-}, the transfer is possible for surface defects such as steps, kinks and vacancies [11]. Bicarbonate formation is also seen on anatase TiO_2 which is very labile [12,13]. No dissociation of CO_2 occurs on anatase TiO_2 [12,14,15]. CO_2 dissociation is seen on Pt/TiO_2 by using FTIR at RT and XPS [16,17]. It is also important to mention here that Pt brings in its own activity to the reaction by efficient adsorption and dissociation of O_2 in the dark than TiO_2, reverse spillover process for hydrogenation, enhancing the activity of OH sites which acts as hole traps [18].

Photocatalytic CO_2 reduction with H_2 [19] is studied on titania and CO and CH_4 evolution have been observed. In the same study, the enhancing effect on CH_4 production is shown when H_2O was added besides H_2 as reactant. Methanation of CO_2 with H_2 has been observed on Ru/TiO_2 at RT and atmospheric pressure which is greatly enhanced with photoirradiation [20]. Photoreduction of CO_2 by H_2 occurred on Rh/TiO_2 under low pressure and RT [21]. Product change has been observed from CO to CH_4 when oxidation state of Rh has changed to metallic state. This was explained by the suppression in the H_2 dissociation ability by Rh in an oxide state [21]. Hydrogen remaining adsorbed on the solid after reduction promotes the dissociation of CO_2 on Rh/TiO_2 [22–24]. On TiO_2 (1 1 0) surfaces, heating of the hydrogenated sample did not lead to recombinative desorption of H_2 (or H_2O) molecules, contrary to the observation over hydroxylated oxide surfaces, but to migration of H atoms into the bulk [25]. Hydrogen molecule spills over on Pt–TiO_2 systems at low temperatures [26]. Hydrogen spillover effect was studied with conductivity measurements [26,27], NMR [28], ESR [29] studies.

Unfortunately, the engineering aspects, yields and selectivities of photocatalytic CO_2 reactions are not as extensively studied due to the slow rates of the reaction requiring primarily batch processes. Furthermore, the photocatalytic CO_2 reduction with H_2O, or artificial photosynthesis, reactions are further hampered by the additional resistances due to the water splitting kinetics. We have reviewed the literature for the photocatalytic water splitting rates as well as CO_2 reduction rates and presented a sample pool of the results in Tables 1 and 2. The immediate conclusion we can draw from the data presented in Tables 1 and 2 is that photocatalytic water splitting reactions have higher rates than CH_4 formation rates. However, this fact has to be taken with some caution: the highest rates observed in photocatalytic water splitting reactions have sacrificial reagents such as MeOH or NaOH in the system thus the true rates of water splitting are a little bit elusive under the reported conditions. Similar to the catalytic CO_2 reduction reaction with H_2 over unpromoted Fe catalysts [4], the primary product of photocatalytic CO_2 reduction reaction with water is methane. A recent report [30] challenges the low production rates of methane formation during artificial photosynthesis reactions. The authors studied the CO_2 reduction rates with ^{13}C labeled CO_2 to observe that formed methane is mostly ^{12}C indicating that the methane evolution was a result of the structural carbon remained in the catalyst from residual organic material of the starting precursor. Although this challenge is genuine, the vast amount of information pouring in the knowledgebase about highly active catalysts operating at low temperatures without illumination cannot be disregarded [1,2].

In this study, we report the carbon deposition over Pt/TiO_2 structures, and the removal rates of the carbon with water and with H_2 under photo driven and thermally driven reaction conditions. Our results indicate that the photocatalytic activation is predominantly required for water splitting reaction and in the presence of gas phase H_2, the methane formation rates from the surface carbon layer are much higher than that observed during the photocatalytic reduction of CO_2 with water.

2. Experimental

2.1. Catalyst preparation

The sol was prepared by mixing $Ti(OC_3H_7)_4$, C_2H_5OH, CH_3COOH, H_2O at the ratio [15:90:1:1], respectively [31]. The solution was mixed for 15 h. The glass beads were dip-coated (dipping rate: 7.5 cm/min – 10 min holding in the solution) 1–3–5 times with the sol, dried at 120 °C and calcined in the end at 450 °C for 5 h. Several layers were coated as such. Pt incorporated into the structure by adding Pt precursor ($Pt(NH_3)_4Cl_2{\cdot}H_2O$) into the solution in 0.1 mol.%. These samples are indicated as (Pt(in)–TiO_2). In addition, for reaction tests in series, Pt was dip-coated on the surface of 5 times coated Pt(in)–TiO_2 glass beads by the same procedure using Pt precursor dissolved in water. These samples are indicated as (Pt(on)–Pt(in)–TiO_2). The samples were further calcined at 450 °C for 5 h for Pt activation.

Table 2
Photocatalytic CO_2 reduction rates.

Photocatalyst	CH_4 production rates (μmol/gTiO_2-h)	CH_4 initial production rates[a] (μmol/gTiO_2-h)	CH_3OH production rates (μmol/gTiO_2-h)	Reductant	Light source	References
1%Rh/TiO_2	–	–	0.53	Water (l)	500 W high pressure Xe lamp	[40]
1%Rh + TiO_2 + 2% WO_3	–	–	3.97	Water (l)	500 W high pressure Xe lamp	[40]
TiO_2 on glass (Vycor®)	0.1[b]	–	0.02	Water (g)	75 W Hg lamp >280 nm	[41]
JRC-TiO-4[c]	0.2	–		Water (g)	75 W Hg lamp >280 nm	[42]
ex[d]-Ti-oxide/Y-zeolite	4.2[b]	6.7	2.78	Water (g)	75 W Hg lamp	[43]
Pt – ex[d]-Ti-oxide/Y-zeolite (1%)	7.3[b]	–	0.53	Water (g)	75 W Hg lamp	[43]
Ti-MCM-48	7.7[b]	–	3.07	Water (g)	Hg lamp	[44]
Pt–Ti-MCM-48 (1%)	12.3[b]	–	0.28	Water (g)	Hg lamp	[44]
Pt–Ti-MCM-48 (0.1%)	9.6[b]	–	1.02	Water (g)	Hg lamp	[44]
Ti-MCM-41	1.8[b]	–	0.8	Water (g)	100 W Hg lamp	[45]
Ti-PS (h,50)[e]	4.3[b]	–	1.13	Water (g)	100 W Hg lamp	[45]
Ti-β(F)[f]	0.4[b]	–	0.31	Water (g)	100 W high pressure Hg lamp	[46,47]
TS-1	0.8[b]	–	0.25	Water (g)	100 W high pressure Hg lamp	[46]
Ti-β(OH)[g]	3.5[b]	–	0.43	Water (g)	100 W high pressure Hg lamp	[46]
P-25	0.2[b]	–	–	Water (g)	100 W high pressure Hg lamp	[46]
TiO_2 on pyrex glass	1.4[a]	1.8	–	H_2	UV light 365 nm	[19]
TiO_2 on pyrex glass	1.7[a]	2.2	–	Water (g)	UV light 365 nm	[19]
TiO_2 on pyrex glass	4.1[a]	16.1	–	Water (g) + H_2	UV light 365 nm	[19]
Ti-SBA-15	63.9[b]	–	16.6	Water (g)	100 W Hg lamp >250 nm	[48]
Cu–Fe (0.5 wt.%)-P25 on glass	0.06	–	–	Water (g)	150 W Hg lamp	[49]
Cu–Fe (0.5 wt.%)-P25 on fiber optic cable	0.9	–	–	Water (g)	150 W Hg lamp	[49]
Cu–Fe (0.5 wt.%)-P25 on fiber optic cable	0.3	–	–	Water (g)	Sun light	[49]
TiO_2 (in pellet form) (P-25)	0.0025[a]	–	–	Water (g)	1.6 W germicidal lamp 253 nm	[50]
TiO_2 coated beads	4.3[a]	5.0	–	Water (g)	150 W Hg lamp	[51]
Pt–TiO_2 coated beads (0.25%)	11.5[a]	17.2	–	Water (g)	150 W Hg lamp	[51]

[a] Converted from line graph using initial data.
[b] Converted from bar graph.
[c] Reference standard catalyst from Catalysis Society of Japan.
[d] Prepared by ion exchange.
[e] PS: pore structure, (h,50):hexagonal structure with a Si/Ti ratio of 50.
[f] Ti-β zeolite synthesized under hydrothermal conditions using F-ions as anions of structure directing agent.
[g] Ti-β zeolite synthesized under hydrothermal conditions using OH-ions as anions of structure directing agent.

2.2. Catalyst characterization

The XRD measurements of the catalysts were performed using Rigaku D/Max 2200 PC X-Ray Diffractometer using Cu-Kα radiation. BET measurements were done with Micromeritics Gemini V Surface Area and Pore Size Analyzer. HR-TEM analysis was performed on a JEOL JEM 2100F field emission gun scanning transmission electron microscope operating at an accelerating voltage of 200 kV using a single tilt holder. Specimen was prepared after scraping the film by a scalpel from the glass substrate as powder, dispersing this powder in ethanol in an ultrasonic bath for 10 min. The solution was dropped on copper grids covered with lacey carbon films.

2.3. Reaction tests

The reaction tests were carried out in a Pyrex manifold (79.7 cm^3) connected to a high vacuum system (10^{-6} Pa range) under batch conditions. Prior to the reaction measurements, H_2 pretreatment was done over the catalyst for 2 h at 220 °C around 250 Torr gas pressure while replacing H_2 gas was replaced every hour. After the reduction the manifold was evacuated and the sample was cooled to room temperature under vacuum. After ensuring that all the gases were evacuated from the manifold, liquid water was injected in the manifold with a syringe through the sampling septum and allowed to evaporate to its vapor pressure ~20 Torr at room temperature. CO_2 gas was introduced into the manifold to bring the total pressure to around 680 Torr. The reaction was allowed to progress under UV light or in dark. The reaction products were collected using a syringe from the gas phase and were analyzed by Varian 3900 GC with FID detector and PoraPLOT Q capillary column at every 30 min. After 2 h of reaction progress, the chamber was evacuated and the fresh gases were introduced. The vacuuming time between runs was kept at 10–15 min. UV irradiation of the catalysts was carried out using a 100-W high pressure Hg lamp (average $\lambda \sim 365$ nm). Due to the heating of the reaction chamber by irradiation, the reaction chamber was at ~80–85 °C. When the gas phase was pure H_2, the chamber pressure was kept at 680 Torr.

3. Results and discussion

The objective or this work was to investigate the CO_2 reduction performance of sol–gel coated TiO_2 films. The effect of Pt metal introduced into the sol–gel structure as well as added on the films by incipient wetness technique was also investigated. In this part, the results of this study and our interpretations for the future material design will be presented.

The crystal structures of the sol–gel coated films with Pt incorporated both in and on the structures monitored by XRD are given in Fig. 1. The XRD data of the films are compared to the XRD struc-

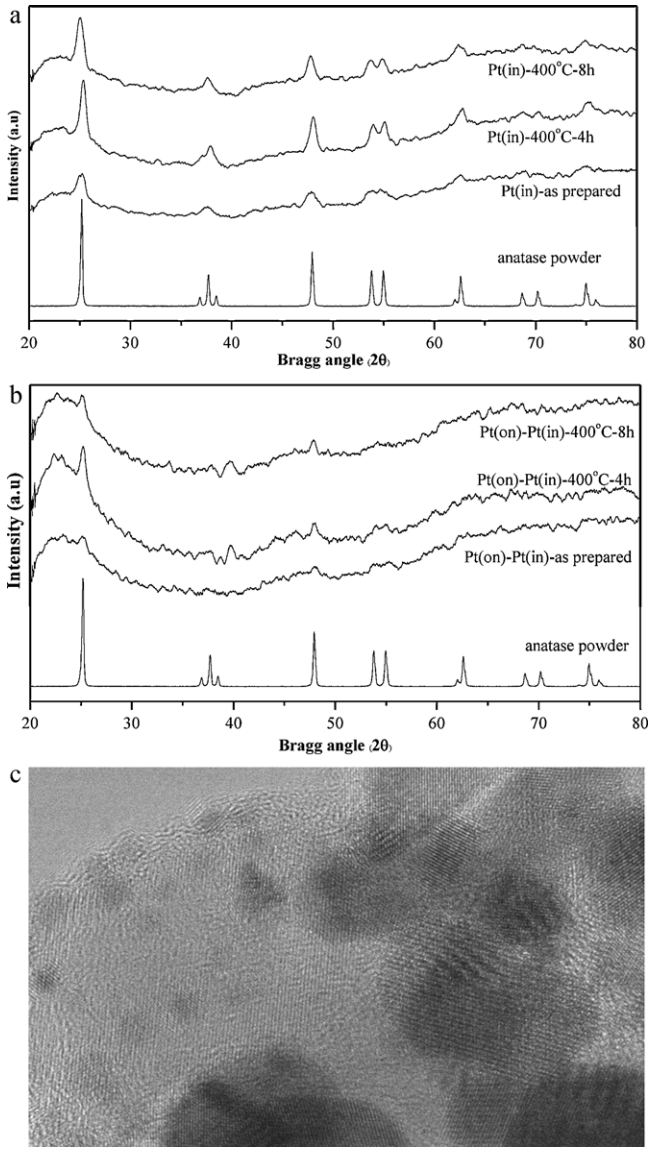

Fig. 1. XRD patterns of the TiO_2 films coated on the glass beads (a) TiO_2 films with Pt incorporated in the sol prior to calcinations, calcined at three stages; (b) the films are further coated with Pt via the incipient wetness technique and (c) the corresponding HR-TEM image containing Pt incorporated via incipient wetness technique.

tures of pure anatase powder. In Fig. 1a TiO_2 films with Pt added in the sol are presented. The pretreatment procedure was definitely not sufficient to form crystalline phases as the increase in the calcination temperatures increased the crystallinity indicated by the increase in the anatase related peaks with increasing duration of the calcination. On the other hand, not much variation in the peaks were observed for the samples when more Pt was added by incipient wetness technique, as seen in Fig. 1b. Due to the low amounts of the samples, the diffraction patterns exhibit very low signal to noise ratio. However, the data can be used to confirm the formation of the anatase phase based on the peaks at $2\theta = 25.28$ and 48.05. The XRD patterns of the samples further calcined for 4 h and 8 h revealed a lack of change, indicating the completion of calcination and the formation of long range order. Furthermore, the lack of change also confirms that the calcination of the samples was sufficient to remove all the organic phase [30] and the formation of TiO_2 phase would not be altered with further calcinations. The HR-TEM image shown in Fig. 1c confirms the crystallinity of the Pt. It is even possible to observe Moire fringes on some of the particles. Furthermore, the crystal planes of TiO_2 are also clearly visible in the image indicating the formation of long range order.

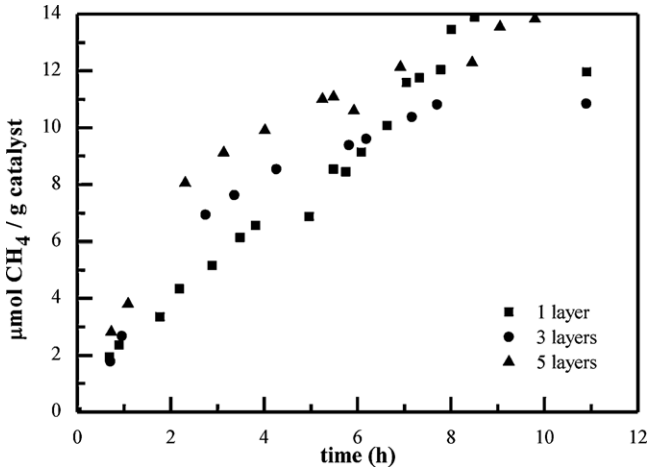

Fig. 2. The photocatalytic methane formation rates from CO_2 and H_2O over pure TiO_2 films. The activities are reported normalized to the amount of the catalyst.

The effect of the film thickness on the activity was tested for pure and Pt containing sol–gel films of TiO_2. The motivation for this part of the study was to investigate the effect of Pt "doped" in the structure on the CO_2 reduction activity of TiO_2 films. In Fig. 2, the results of film thickness on the catalytic activity under photocatalytic water reduction of CO_2 were presented. The reaction rates were presented normalized to the amount of the catalyst presented. It was observed that the methane evolution rates did not change much when the film thicknesses were increased. The results are interpreted as the formation of a tortuous TiO_2 structure such that the lower layers were accessible to illumination and also to chemical conversion.

When Pt(in) samples were tested for photocatalytic CO_2 reduction reaction with H_2O, it was observed that the activity of the films with one layer of coating was greater than the other samples (Fig. 3). In fact, a systematic decrease of the methane formation rates was observed with increasing film thickness. This was interpreted as Pt catalyzed crystallization of the TiO_2 structures. The tortuous framework observed in the pure films was no longer present. The BET analysis of the films revealed that the Pt containing films indeed had lower surface areas (Table 3).

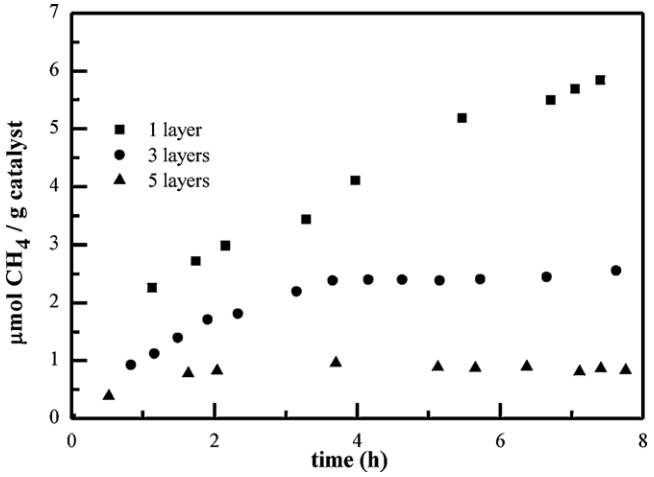

Fig. 3. The photocatalytic methane formation rates from CO_2 and H_2O over TiO_2 films containing Pt in the structure. The activities are reported normalized to the amount of the catalyst.

Table 3
Photocatalytic CO_2 reduction rates obtained in this study along with the specific surface areas of the samples.

Catalyst	BET surface area (m^2/g)	Rate (μmol/g_{cat}-h)
TiO_2-1 layer	–	2.05
TiO_2-3 layer	49	2.55
TiO_2-5 layer	63	3.50
Pt–TiO_2-1 layer	–	1.53
Pt–TiO_2-3 layer	43	0.94
Pt–TiO_2-5 layer	29	0.44

After this point, it was decided to look for the methane formation mechanisms over the samples which had the most dense structure. The sample with Pt incorporated in the TiO_2 sol with further Pt added via incipient wetness technique was chosen for further study. The sample was exposed to different gas atmospheres and the results of the photocatalytic methane production reaction are presented in Fig. 4. There are three different reaction zones, and the vertical dotted lines indicate evacuating the system and replenishing the gas phase atmosphere. In the first reaction zone, CO_2 reduction with water vapor was followed. The deactivation of the catalyst could be followed by the activity loss with each subsequent gas replenishment. In the second reaction zone, only gas phase H_2 was provided and the reaction products with respect to time was followed. In this zone, no carbon source was available except the carbon deposited on the surface most probably in the form of a surface carbonate. It is clear that the rate of methane formation was much faster, and a significant amount of methane was formed during this reaction zone. After the methane formation rates decreased to that of the fresh catalyst, the system was evacuated and pure CO_2 was delivered in the reaction chamber with no source of hydrogen (third reaction zone). In this zone significant formation of methane was still observed, due to the presence of spilled over hydrogen over TiO_2 surface.

In order to demonstrate that the hydrogen spilled over from the metal to TiO_2, the fresh catalyst was reduced with hydrogen followed by a brief evacuation period ensuring that spilled over hydrogen is not removed from the catalyst (10 min, in this system) [28]. Subsequently, CO_2 was sent to the chamber, and the kinetics of the methane formation was monitored. The results are presented in Fig. 5. The follow up figures indicate the presence of only one reactant (CO_2 or H_2), and the other reactant is present in the system as a surface intermediate. In the first step, the spilled over hydrogen over the support is used to reduce CO_2. In the second step, we observe a very high rate of methane formation. Methane forms from the carbon containing intermediate over the surface via the hydrogen adsorbed on the surface from the gas phase. After 1 h of monitoring the kinetics, the system was evacuated and fresh hydrogen was fed to the system. The decrease in the methane formation rates upon each hydrogen dose was due to the depletion of the carbon intermediate over TiO_2 surface. In the last frame, the system was dosed with pure CO_2 and methane formation kinetics from spilled over hydrogen was monitored. It is important to note that the methane formation rates in the first and the last steps are

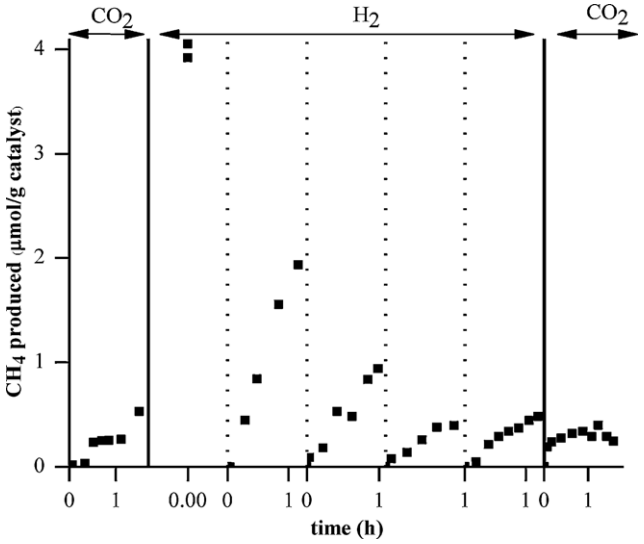

Fig. 5. Methane formation rates under different reaction conditions: first frame: methane formation from residual hydrogen on the surface from reduction and gas phase CO_2; next five frames: methane production from surface carbon intermediate and gas phase hydrogen; last frame: methane formation from surface hydrogen and gas phase CO_2.

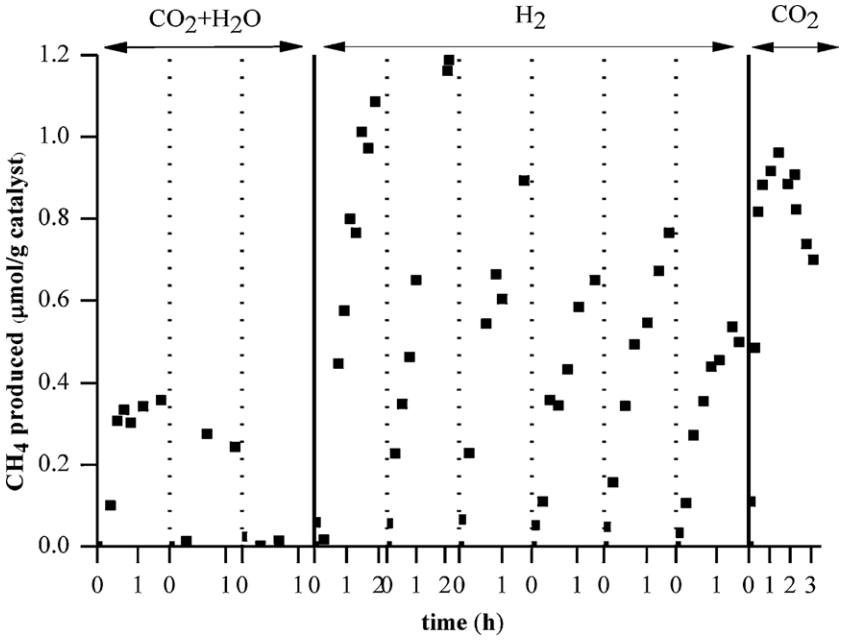

Fig. 4. Methane formation rates under different reaction conditions: first three frames: artificial photosynthesis conditions; next six frames: methane formation from the surface carbon and gas phase hydrogen; last frame: methane formation from surface spilled over hydrogen and gas phase CO_2.

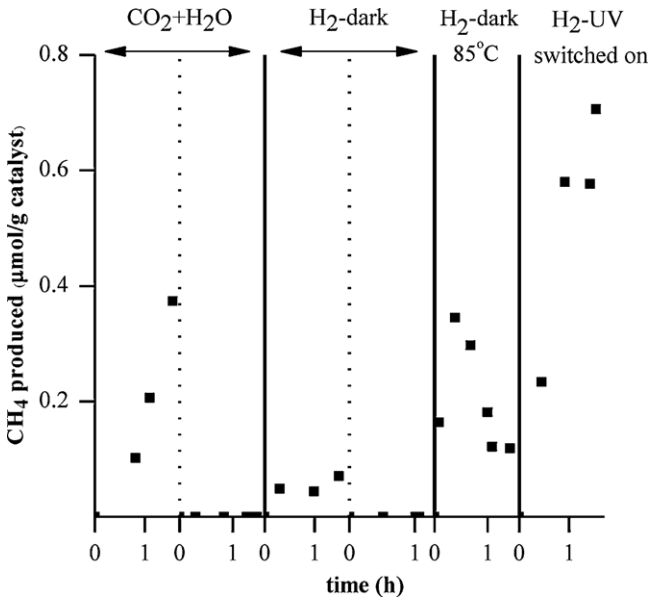

Fig. 6. Dark kinetics of methane formation after artificial photosynthesis conditions: first two frames: UV irradiated $CO_2 + H_2O$ reactants; next two frames: methane production in dark from surface carbon intermediate and gas phase hydrogen; 5th frame: methane production in dark at 85 °C from surface carbon intermediate and gas phase hydrogen; last frame: methane production from surface carbon intermediate and gas phase hydrogen under UV illumination.

similar indicating that the activity of the catalyst was not altered during the tests.

Finally, the dark reaction kinetics of CO_2 reduction with hydrogen was followed. For this purpose, the surface of the catalyst was populated with the carbon containing intermediate by exposing $CO_2 + H_2O$ mixture twice and irradiated under UV for 1 h each and methane formation kinetics were monitored (Fig. 6). After establishing that the surface is coated with carbon containing intermediate, the dark reaction kinetics upon hydrogen exposure was followed. Methane formation was observed, but the rates were lower than that observed under UV irradiation (Fig. 5) and the activity was lost immediately. The effect of temperature was also monitored by setting the temperature to 85 °C and higher rates of methane formation was observed in the dark. It should be noted that the methane formation rates exhibited a peak during these tests which needs further exploration of the surface reaction mechanism. In the last step of the measurements, the methane formation rates were monitored in the presence of hydrogen gas only and under UV irradiation. The rates under UV irradiation are much higher than the dark reaction kinetics indicating a thermal and a photocatalytic component of the surface carbon containing intermediate hydrogenation.

All of these experiments indicated that during the photocatalytic reduction of CO_2 with water, a significant carbon containing intermediate deposition took place. The carbon containing intermediate deposition started as surface HCO_3^- formed from CO_2 and surface OH groups [13]. Once dissociated hydrogen is available, the surface intermediate was immediately converted to methane. Hydrogen is present over the surface as spilled over form, and it can resist evacuation due to the surface diffusion resistance [28]. These results present a different perspective and can be used to design photocatalytic CO_2 reduction systems.

The results presented in this study reveal striking similarities between natural and artificial photosynthesis systems. The experiments intended to elucidate the mechanism of reduction of CO_2 with H_2O over TiO_2 surfaces revealed that it was very easy to accommodate CO_2 on basic TiO_2 structures. CO_2 was essentially titrating the OH groups present over TiO_2 and forming HCO_3^- structures similar to the accommodation of the CO_2 via the CAM (Crassulacean Acid Metabolism) in Cacti and succulent plants.

There are two important steps in the artificial (and natural) photosynthesis systems. One is the activation of CO_2 and the other one is the activation of H_2O. The data presented above clearly indicated that the adsorption and accommodation of CO_2 is not limiting the rate of methane formation. On the other hand, production of protons and electrons, or hydrogen atoms, is the rate limiting step in the overall process. As can be seen from the data compiled from the literature, the rates of methane formation are close to the rates of photocatalytic water splitting in neutral conditions when no sacrificial agents (such as methanol) are present. It is also important to note that the photocatalytic water splitting rates are still 6–7 orders of magnitude behind the rates of water splitting in the photosynthetic cells [32]. Thus, while there is a huge room for improvement of the artificial photosynthesis mechanisms, the role of the surface and interface transport mechanisms in enhancing the rates and selectivities towards glucose in the photosynthesis is still waiting to be explored for designing efficient artificial photosynthesis systems.

4. Conclusions

Photocatalytic reduction of CO_2 with H_2O was limited by the rates of water splitting reaction, similar to the natural photosynthesis. Carbon deposition over the photocatalyst surface was identified, which could be removed by a hydrogen dose, indicating that the carbon was in partially hydrogenated form. Spilled over hydrogen was responsible for the final hydrogenation step. Furthermore, in the presence of gas phase hydrogen, significant dark activity was also present.

Acknowledgements

This work was supported by TUBITAK under research grant nos: 106Y075 and 107M447. Scholarship for MMO from SANTEZ program in collaboration with Kalekim and Turkish Ministry of Industry and Trade under grant no 00336.STZ.2008-2 is kindly appreciated. The authors are grateful to METU Central Laboratory and Prof. H.J. Kleebe, Mathis M. Muller, Margarete Schlosser for TEM analysis.

References

[1] S. Sharma, Z.P. Hu, P. Zhang, E.W. McFarland, H. Metiu, J. Catal. 278 (2011) 297.
[2] C.Y. Hao, S.P. Wang, M.S. Li, L.Q. Kang, X.B. Ma, Catal. Today 160 (2011) 184.
[3] C. Schild, A. Wokaun, R.A. Koeppel, A. Baiker, J. Phys. Chem. 95 (1991) 6341.
[4] T. Riedel, M. Claeys, H. Schulz, G. Schaub, S.S. Nam, K.W. Jun, M.J. Choi, G. Kishan, K.W. Lee, Appl. Catal. A – Gen. 186 (1999) 201.
[5] T. Riedel, G. Schaub, K.-W. Jun, K.-W. Lee, Ind. Eng. Chem. Res. 40 (2001) 1355.
[6] J.S. Kim, S. Lee, S.B. Lee, M.J. Choi, K.W. Lee, Catal. Today 115 (2006) 228.
[7] S.C. Lee, J.S. Kim, W.C. Shin, M.J. Choi, S.J. Choung, J. Mol. Catal. A – Chem. 301 (2009) 98.
[8] H. Kusama, K.K. Bando, K. Okabe, H. Arakawa, Appl. Catal. A – Gen. 197 (2000) 255.
[9] V.P. Indrakanti, J.D. Kubicki, H.H. Schobert, Energy Environ. Sci. 2 (2009) 745.
[10] M.A. Henderson, Surf. Sci. 400 (1998) 203.
[11] V.P. Indrakanti, H.H. Schobert, J.D. Kubicki, Energy Fuel 23 (2009) 5247.
[12] G. Ramis, G. Busca, V. Lorenzelli, Mater. Chem. Phys. 29 (1991) 425.
[13] K. Tanaka, J.M. White, J. Phys. Chem. 86 (1982) 4708.
[14] J. Rasko, F. Solymosi, J. Phys. Chem. 98 (1994) 7147.
[15] J. Rasko, Catal. Lett. 56 (1998) 11.
[16] K. Tanaka, J.M. White, J. Phys. Chem. 86 (1982) 3977.
[17] K. Tanaka, K. Miyahara, I. Toyoshima, J. Phys. Chem. 88 (1984) 3504.
[18] D. Uner, The effect of addition of Pt on the gas phase photocatalysis over TiO_2 , in: M. Anpo, P.V. Kamat (Eds.), Environmentally Benign Photocatalysts: Application of Titanium Oxide Based Materials, Springer, New York, 2010, pp. 479–502.
[19] C.C. Lo, C.H. Hung, C.S. Yuan, J.F. Wu, Sol. Energy Mater. Sol. Cells 91 (2007) 1765.
[20] K.R. Thampi, J. Kiwi, M. Gratzel, Nature 327 (1987) 506.

[21] Y. Kohno, H. Hayashi, S. Takenaka, T. Tanaka, T. Funabiki, S. Yoshida, J. Photochem. Photobiol. A 126 (1999) 117.
[22] F. Solymosi, A. Erdohelyi, T. Bansagi, J. Chem. Soc. Faraday Trans. I 77 (1981) 2645.
[23] M.A. Henderson, S.D. Worley, J. Phys. Chem. 89 (1985) 1417.
[24] M.L. McKee, C.H. Dai, S.D. Worley, J. Phys. Chem. 92 (1988) 1056.
[25] X.L. Yin, M. Calatayud, H. Qiu, Y. Wang, A. Birkner, C. Minot, C. Woll, Chemphyschem 9 (2008) 253.
[26] U. Roland, R. Salzer, T. Braunschweig, F. Roessner, H. Winkler, J. Chem. Soc. Faraday Trans. 91 (1995) 1091.
[27] U. Roland, T. Braunschweig, F. Roessner, J. Mol. Catal. A – Chem. 127 (1997) 61.
[28] D.O. Uner, M. Pruski, T.S. King, J. Catal. 156 (1995) 60.
[29] T.M. Salama, H.K. Ebitani, H. Hattori, H. Kita, Chem. Mater. 6 (1994) 21.
[30] C.C. Yang, Y.H. Yu, B. vander Linden, J.C.S. Wu, G. Mul, J. Am. Chem. Soc. 132 (2010) 8398.
[31] K. Hayek, R. Kramer, Z. Paal, Appl. Catal. A – Gen. 162 (1997) 1.
[32] D. Uner, M.M. Oymak, B. Ipek, Int. J. Global Warming 3 (2011) 142.
[33] E.A. Kozlova, T.P. Korobkina, A.V. Vorontsov, V.N. Parmon, Appl. Catal. A – Gen. 367 (2009) 130.
[34] R. Dholam, N. Patel, M. Adami, A. Miotello, Int. J. Hydrogen Energy 34 (2009) 5337.
[35] K. Yamaguti, S. Sato, J. Chem. Soc. Faraday Trans. I 81 (1985) 1237.
[36] R. Abe, K. Sayama, K. Domen, H. Arakawa, Chem. Phys. Lett. 344 (2001) 339.
[37] O. Rosseler, M.V. Shankar, M.K.L. Du, L. Schmidlin, N. Keller, V. Keller, J. Catal. 269 (2010) 179.
[38] G.L. Chiarello, E. Selli, L. Forni, Appl. Catal. B – Environ. 84 (2008) 332.
[39] Y.Z. Yang, C.H. Chang, H. Idriss, Appl. Catal. B – Environ. 67 (2006) 217.
[40] F. Solymosi, I. Tombacz, Catal. Lett. 27 (1994) 61.
[41] M. Anpo, K. Chiba, J. Mol. Catal. 74 (1992) 207.
[42] M. Anpo, H. Yamashita, Y. Ichihashi, S. Ehara, J. Electroanal. Chem. 396 (1995) 21.
[43] M. Anpo, H. Yamashita, Y. Ichihashi, Y. Fujii, M. Honda, J. Phys. Chem. B 101 (1997) 2632.
[44] M. Anpo, H. Yamashita, K. Ikeue, Y. Fujii, S.G. Zhang, Y. Ichihashi, D.R. Park, Y. Suzuki, K. Koyano, T. Tatsumi, Catal. Today 44 (1998) 327.
[45] I. Keita, S. Nozaki, M. Ogawa, M. Anpo, Catal. Today 74 (2002) 241.
[46] M. Kitano, M. Matsuoka, M. Ueshima, M. Anpo, Appl. Catal. A – Gen. 325 (2007) 1.
[47] K. Ikeue, H. Yamashita, M. Anpo, T. Takewaki, J. Phys. Chem. B 105 (2001) 8350.
[48] J.S. Hwang, J.S. Chang, S.E. Park, K. Ikeue, M. Anpo, Top. Catal. 35 (2005) 311.
[49] T.V. Nguyen, J.C.S. Wu, C.H. Chiou, Catal. Commun. 9 (2008) 2073.
[50] S.S. Tan, L. Zou, E. Hu, Sci. Technol. Adv. Mater. 8 (2007) 89.
[51] O. Ozcan, F. Yukruk, E.U. Akkaya, D. Uner, Appl. Catal. B – Environ. 71 (2007) 291.